



Article

Chronic Inhibition of Nitric Oxide Synthases Impairs Spatiotemporal Learning and Memory to a Similar Extent in C57BL/6 and hAPP23+/- Mice

Jhana O. Hendrickx ¹, Elke Calus ², Peter Paul De Deyn ^{2,3}, Debby Van Dam ^{2,3} and Guido R. Y. De Meyer ^{1,*}

¹ Laboratory of Physiopharmacology, University of Antwerp, Wilrijk, 2610 Antwerp, Belgium

² Laboratory of Neurochemistry and Behaviour, Experimental Neurobiology Unit, Wilrijk, 2610 Antwerp, Belgium; elke.calus@uantwerpen.be (E.C.); peter.dedeyn@uantwerpen.be or p.p.de.deyn@umcg.nl (P.P.D.D.); debby.vandam@uantwerpen.be (D.V.D.)

³ Department of Neurology and Alzheimer Center Groningen, University Medical Center Groningen, University of Groningen, 9713 AV Groningen, The Netherlands

* Correspondence: guido.demeyer@uantwerpen.be

Abstract: Due to global population growth, age-related disorders like cardiovascular disease and dementia are anticipated to increase. Recent data suggests a connection between cardiovascular disease and neurodegeneration, especially focusing on arterial stiffness (AS) and Alzheimer’s disease (AD). In light of this, we conducted a study to explore the impact of long-term nitric oxide synthase (NOS) isoform inhibition, which leads to AS, on neurobehavioral performance. We also compared these effects in an AD model and control mice. C57BL/6 and hAPP23+/- mice (an established AD model) were given 0.5 mg/mL N(G)-Nitro-L-Arginine Methyl Ester (L-NAME) in their drinking water for 16 weeks. Our findings indicate that chronic non-selective NOS inhibition increased AS and reduced spatiotemporal learning and memory in both C57BL/6 and hAPP23+/- mice. These effects were consistent across both groups, emphasizing the role of neuronal NOS (nNOS) in cognitive aging, regardless of genetic predisposition to AD.

Keywords: arterial stiffness; Alzheimer’s disease; nitric oxide; learning and memory; amyloid



Citation: Hendrickx, J.O.; Calus, E.; De Deyn, P.P.; Van Dam, D.; De Meyer, G.R.Y. Chronic Inhibition of Nitric Oxide Synthases Impairs Spatiotemporal Learning and Memory to a Similar Extent in C57BL/6 and hAPP23+/- Mice. *Int. J. Transl. Med.* **2023**, *3*, 516–526. <https://doi.org/10.3390/ijtm3040036>

Academic Editor: Francesco Fornai

Received: 25 September 2023

Revised: 27 November 2023

Accepted: 12 December 2023

Published: 14 December 2023



Copyright: © 2023 by the authors. Licensee MDPI, Basel, Switzerland. This article is an open access article distributed under the terms and conditions of the Creative Commons Attribution (CC BY) license (<https://creativecommons.org/licenses/by/4.0/>).

1. Introduction

In the past, cardiovascular disease and neurodegeneration were traditionally regarded as distinct medical conditions, categorized based on well-established clinical criteria. However, recent epidemiological research has challenged this notion by uncovering shared mechanisms between these two pathological conditions. Particularly, arterial stiffness (AS) has emerged as a significant risk indicator for brain aging and the onset of Alzheimer’s disease (AD) [1–3]. AS plays a pivotal role in transmitting cardiac pulsations to the brain. Given the brain’s intricate microvascular network, it not only exhibits low resistance but also sustains continuous exposure to pulsatile pressures and mechanical forces from the heart [4]. It is widely accepted that an increase in pulse wave velocity (PWV), an in vivo AS marker, is associated with AD-related symptoms, including accelerated cognitive decline, alterations in psychomotor speed, and difficulties in semantic fluency and verbal learning [1,2,5]. Additionally, imaging-based studies conducted in both symptomatic and asymptomatic individuals have highlighted the link between elevated PWV measurements and structural brain changes such as cerebrovascular damage, increased amyloid- β (A β) burden, and cerebral amyloid angiopathy [6–9].

While the growing body of epidemiological evidence suggests a mechanistic overlap, it is essential to acknowledge its correlational nature, emphasizing the imperative need for more targeted research. In this context, animal models of arterial stiffness serve as

valuable tools for investigating the causal mechanisms that connect these two pathological conditions.

Previous research findings strongly support the pivotal role of nitric oxide (NO), particularly neuronal nitric oxide synthase (nNOS), in the pathophysiology of both cardiovascular and neurological conditions. These contributions are significant in understanding the convergence between AS and the acceleration of brain aging [10]. NO is well-established in the contexts of AS [10,11] and AD [12–14], primarily due to its involvement in nitro-oxidative stress. The connection between AS and AD has largely been associated with maintaining blood-brain barrier integrity [15,16] and the role of endothelial NO in amyloidogenic processing of amyloid precursor protein (APP) within human and rodent cerebrovasculature [14,17]. However, the precise role of NO in the mechanistic interplay between AS and AD remains a topic of debate, necessitating further research to arrive at a more conclusive understanding. In this study, our objective was to further investigate the impact of AS induction through chronic non-selective inhibition of all NOS activity on the progression of AD in a well-characterized humanized heterozygous APP overexpressing (hAPP23+/-) mouse model.

2. Materials and Methods

2.1. Experimental Set-Up

All male mice were housed in standard mouse cages with a maximum of eight animals per cage, following conventional laboratory conditions. These conditions included a constant room temperature of 22 ± 2 °C, humidity maintained at $55 \pm 5\%$, and a 12-h artificial day/night cycle with lights on at 8 a.m. Food and water were available ad libitum. To achieve NOS inhibition, male hAPP23+/- mice [18] (control n = 9; treated n = 6) and their C57BL/6 littermates (control n = 10; treated n = 6) were provided with drinking water containing 0.5 mg/mL of N(G)-Nitro-L-Arginine Methyl Ester (L-NAME) starting at 8 weeks of age and continued for 16 weeks. This regimen aimed to achieve partial inhibition of eNOS (endothelial nitric oxide synthase) activity in the aortic vessel wall, using a lower L-NAME dosage compared to previous studies [19,20]. The animal selection was randomized within each experimental subgroup. To monitor L-NAME intake, the drinking bottles were weighed at the beginning and end of each week, and the L-NAME drinking water was replenished accordingly. The average L-NAME intake for treated mice over the 16-week treatment period was 3.3 ± 0.3 mg per day per animal.

A two-week experimental series followed 15 weeks of L-NAME treatment. In the first week, during the 15th week of treatment, spatial learning and memory were assessed using the Morris Water Maze (MWM) test. In the second week, corresponding to the 16th week of treatment, blood pressure and echocardiographic analyses were performed. At week 16, the mice were euthanized under deep anesthesia with sodium pentobarbital (250 mg/kg, i.p. [21]) to allow ex vivo assessment of arterial stiffness and histological analysis of cerebral amyloidosis. The experiments were approved by the Animal Ethics Committee of the University of Antwerp (ECD approval n° 2017/53) and were conducted in accordance with the U.K. Animals (Scientific Procedures) Act, 1986, along with associated guidelines, and EU Directive 2010/63/EU for animal experimentation. Furthermore, these experiments were conducted in compliance with the ARRIVE (Animal Research: Reporting of In Vivo Experiments) Guidelines [22].

2.2. Spatiotemporal Learning and Memory

At 6 months of age, all animal groups were assessed for spatiotemporal learning and memory, including C57BL/6, L-NAME treated C57BL/6, hAPP23+/-, and L-NAME treated hAPP23+/-, using the MWM test [23,24]. This test involved a 150 cm diameter circular pool, 30 cm high, filled with opaque water at 25 °C. Visual cues were strategically placed around the pool. The MWM test had two main phases: the acquisition phase and the probe trial. Over 4 days, the acquisition phase included two daily trial blocks with four trials each, conducted at 10:30 a.m. and 03:00 p.m., with a 15-min inter-trial interval.

Mice had to find a submerged platform within 120 s. In case they did not, they were guided to the platform and stayed for 15 s before returning to their home cage. The starting positions varied randomly. Four days after the acquisition phase, the probe trial took place. The platform was removed, and the mice were released in a fixed quadrant position. Their swimming paths were recorded for 100 s. A computerized video-tracking system (Ethovision, Noldus, The Netherlands) recorded data, including path length, escape latency, swimming speed, and the percentage of time spent in each quadrant during the acquisition phase to assess spatial accuracy. Importantly, experimenters were blinded to the genetic or treatment status of the mice throughout these trials.

2.3. Blood Pressure Measurements

Peripheral blood pressure was non-invasively measured using the CODA tail-cuff blood pressure system (KENT Scientific CO., Torrington, CT, USA), following previously established procedures [25]. The mice were gently secured in a plexiglas holder, and occlusion and volume pressure cuffs were carefully placed around the tail. The voltage output from both cuffs was systematically recorded and subsequently analyzed using a PowerLab signal transduction unit in conjunction with associated graph software (ADInstruments, Oxford, UK). To enhance measurement reliability and minimize any potential discomfort to the animals, blood pressure readings were obtained two days prior to the main measurement, with the actual measurements being conducted on the third day. Each measurement session comprised 15 cycles, taking approximately 15 min per animal. The reported values represent the mean values obtained on the third day.

2.4. Echocardiography and PWV Measurements

Echocardiography and PWV measurements were performed using a high-resolution digital imaging system (Vevo® 2100 Imaging System, FUJIFILM Visual Sonics Inc., Toronto, ON, Canada). A high-frequency transducer probe (Visual Sonics MS500D, FUJIFILM Visual Sonics, Inc., Toronto, Canada) with a frequency range of 18–38 MHz was used to assess systolic and diastolic heart function in mice. Mice were anesthetized and placed on a preheated platform in a supine position to maintain their body temperature at 36–38 °C. Body temperature was monitored using an anal thermometer probe and isoflurane concentrations were adjusted to maintain heart rate at 500 ± 50 bpm. Systolic left ventricular dimensions were measured using short-axis M-mode images and used to calculate fractional shortening (FS%) and ejection fraction (EF%). Diastolic cardiac function was assessed using color and pulse wave Doppler recordings of the trans-tricuspid flow. Cardiac parameters were reported as the mean of three consecutive M-mode and/or pulse wave Doppler images. PWV measurements of the abdominal aorta (aPWV) were performed on anesthetized mice using a 24-MHz transducer (Visual Sonics MS400, FUJIFILM Visual Sonics, Inc., Toronto, Canada) and the method developed by Di Lascio et al. [26]. B-mode images of the abdominal aorta were obtained to measure aortic diameter (D) and pulse wave Doppler tracing was used to measure aortic flow velocity (V). The slope of the linear part of the resulting ln(D)-V loop was used to calculate PWV values using Matlab v2014 (Mathworks, Natick, MA, USA). Body temperature was maintained at 36–38 °C and heart rates were kept at 500 ± 50 bpm by adjusting isoflurane concentrations.

2.5. Rodent Oscillatory Tension Set-Up for Arterial Compliance (ROTSAC)

After the mice were humanely killed, the thoracic aorta was removed and cleared of surrounding tissue. The descending thoracic aorta was cut into six 2 mm segments, starting 2 mm distal to the aortic arch, for vascular reactivity and stiffness analyses. These segments were placed in Krebs Ringer solution and aerated with a 95% O₂/5% CO₂ gas mixture to maintain pH at 7.4. Aortic segments were mounted in organ baths filled with KR solution and diameter and transmural pressure were estimated using the Laplace relationship. Force and displacement were measured with a force-length transducer connected to a data acquisition system. The Peterson Modulus (Ep) was calculated using the formula

$E_p = D_0 \times (\Delta P / \Delta D)$, where ΔD is the difference between systolic and diastolic diameter, ΔP is the pressure difference of 40 mmHg, and D_0 is the diastolic diameter. A pulse pressure difference of 40 mmHg was applied at a frequency of 10 Hz, corresponding to a physiological heart rate of 600 bpm in mice. Measurements took an average of 5–10 min.

2.6. Histology

Brain tissue was collected and fixed in a 4% formalin solution for 24 h. The tissue was then dehydrated using 60% isopropanol and embedded in paraffin. Serial cross-sections of the hippocampal and cortical brain tissue were prepared for histological analysis. The slides were deparaffinized by transferring them through 100% alcohol twice for 3 min, followed by 95%, 70%, and 50% alcohol for 3 min each. Endogenous peroxidase activity was blocked by incubating the sections in a 3% hydrogen peroxide solution in methanol for 10 min. The slides were then rinsed twice in PBS for 5 min and subjected to antigen retrieval using 88% formic acid for 20 min at room temperature. The tissue sections were then treated with a primary antibody against β -amyloid, diluted 1:200, and incubated at 4 °C overnight. The following day, the slides were washed twice in PBS for 5 min and a biotinylated secondary antibody was added to the sections, followed by incubation in a humidified chamber at room temperature for 30 min. The slides were then washed twice in PBS for 5 min and streptavidin-HRP conjugates were added to the sections for 30 min in a humidified chamber at room temperature, protected from light. The slides were then washed twice in PBS for 5 min and a freshly made diaminobenzidine solution was applied to the sections. The slides were then washed twice in PBS for 5 min, counterstained with hematoxylin for 1–2 min, washed in running tap water for more than 15 min and dehydrated through four changes of alcohol (95%, 95%, 100%, and 100%) for 5 min each before being mounted. Microscopic images were obtained using an Olympus BX4 microscope with Universal Grap 6.1 software and quantified using ImageJ software. Cerebral amyloidosis was analyzed by measuring the percentage area fraction of positively stained hippocampal and cortical (parietal and occipital cortex) microscopic images.

2.7. Statistical Analysis

The data are presented as the mean \pm standard error of the mean unless otherwise specified. A factorial analysis of variance (ANOVA) was conducted with the factor's 'treatment', 'genotype', and the interaction between 'treatment' and 'genotype'. A *p*-value of less than 0.05 was considered statistically significant. For the MWM probe trial, statistics were calculated using a factorial ANOVA with the factors 'Quadrant \times treatment', 'Quadrant \times genotype', and the interaction between 'Quadrant \times treatment \times genotype', as well as via Dirichlet distributions, as previously described [27]. The statistical analyses used are indicated in the figure legends and were performed using GraphPad Prism software (v. 8.0.0 for Windows, GraphPad Software, San Diego, CA, USA).

3. Results

3.1. L-NAME Treatment Does Not Affect Peripheral Blood Pressure

No effect of L-NAME treatment, genotype, and the combined effect of the L-NAME treatment and genotype could be observed for systolic (Figure 1A), diastolic (Figure 1B) and pulse pressure measurements (Figure 1C) in both hAPP23+/- and C56BL/6 mice.

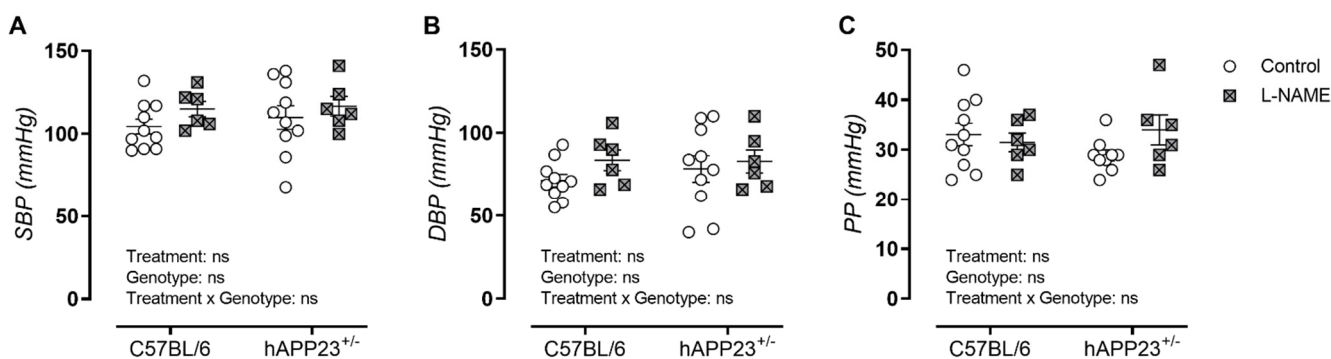


Figure 1. Peripheral blood pressure measurements. (A). Systolic blood pressure (SBP), (B). diastolic blood pressure (DBP) and (C). pulse pressures (PP) of (non)treated hAPP23^{+/-} mice (control: n = 9; treated: n = 6) and respective C57BL/6 littermates (control: n = 10; treated: n = 6). Factorial ANOVA for the factor's 'Treatment', 'Genotype' and 'Treatment × Genotype'. Non-significant results are indicated as 'ns'. Data are presented as mean ± SEM.

3.2. L-NAME Treatment Affects Systolic Cardiac Function in hAPP23^{+/-} and C57BL/6 Mice

Echocardiography revealed signs of hypertrophic cardiomyopathy in L-NAME treated hAPP23^{+/-} and C57BL/6 mice through a tendency toward increased left ventricular inner diameters (LVID) and left ventricular posterior wall thicknesses (LVPW) and decreased ejected left ventricular (LV) volumes (Table 1). In addition, trends toward increased left ventricular EF and FS measurements were observed (Table 1). L-NAME treatment did not affect diastolic heart function. However, L-NAME treated hAPP23^{+/-} mice showed increased isovolumetric retention time (IVRT) measurements compared to (un)treated C57BL/6 animals (Table 1).

Table 1. Systolic and diastolic echocardiographic analysis. The p-value columns indicate the factorial effect of 'treatment', 'genotype' and 'treatment × genotype' as calculated with a Factorial ANOVA (* p < 0.05, ** p < 0.01, **** p < 0.0001) with a Tukey post-hoc test for differences between control and L-NAME groups per genotype. Non-significant results are indicated as 'ns'. Data are presented as mean ± SEM. IVS,d = inner ventricular septum thickness during diastole, LVID,d = left ventricular inner diameter during diastole, LVPW,d = left ventricular posterior wall thickness during diastole, LV mass/BW = left ventricular mass corrected for body weight, EF = ejection fraction, FS = fractional shortening, E/A = peak velocity blood flow in early diastole (E) to peak velocity flow in late diastole (A), E/E' = mitral peak velocity of early filling (E) to early diastolic mitral annular velocity (E'), IVRT = isovolumetric retention time.

	C57BL/6		hAPP23 ^{+/-}		<i>p</i> _{treatment}	<i>p</i> _{genotype}	<i>p</i> _{treatment×genotype}
	Control (n = 10)	L-NAME (n = 6)	Control (n = 9)	L-NAME (n = 6)			
Heart weight (mg)	144 ± 4	155 ± 7	154 ± 8	138 ± 4	ns	ns	*
Heart weight (%)	0.5 ± 0.1	0.6 ± 0.1	0.5 ± 0.1	0.5 ± 0.1	ns	ns	ns
IVS,d (mm)	1.0 ± 0.1	1.0 ± 0.1	1.0 ± 0.1	1.0 ± 0.1	ns	ns	ns
LVID,d (mm)	3.4 ± 0.1	3.0 ± 0.2	3.4 ± 0.1	3.2 ± 0.2	0.06	ns	ns
LVPW,d (mm)	1.1 ± 0.1	1.3 ± 0.1	0.9 ± 0.1	1.0 ± 0.1	0.08	**	ns
LV mass (mg)	125 ± 7	134 ± 12	127 ± 7	122 ± 11	ns	ns	ns
LV mass/BW (10 ⁻³)	4.4 ± 0.3	4.9 ± 0.4	4.5 ± 0.2	4.7 ± 0.4	ns	ns	ns
LV volume,d (µL)	48 ± 4	37 ± 4	49 ± 4	43 ± 5	0.06	ns	ns
Stroke volume (µL)	39 ± 3	31 ± 4	36 ± 2	34 ± 3	ns	ns	ns
EF (%)	75 ± 4	86 ± 3	75 ± 3	80 ± 3	0.05	ns	ns
FS (%)	45 ± 4	54 ± 4	43 ± 2	48 ± 3	0.06	ns	ns
E/A (none)	1.6 ± 0.1	1.5 ± 0.2	1.4 ± 0.1	1.3 ± 0.1	ns	ns	ns
E/E' (none)	28 ± 5	29 ± 7	28 ± 3	24 ± 4	ns	ns	ns
IVRT (ms)	15 ± 1	14 ± 1	20 ± 1	22 ± 2	ns	****	ns
Deceleration (ms)	19 ± 2	16 ± 2	18 ± 2	15 ± 1	ns	ns	ns

3.3. L-NAME Treatment Affects AS In Vivo and Ex Vivo in hAPP23+/- and C57BL/6 Mice

A significant effect of the L-NAME treatment was observed in the in vivo and ex vivo AS assessments by means of significantly increased aPWV and Ep measurements in both genotypes (Figure 2A,B). More specifically, aPWV measurements of L-NAME treated animals were significantly increased within each genotypic group (Figure 2A), whereas only a statistical treatment effect was observed for Ep measurements (Figure 2B).

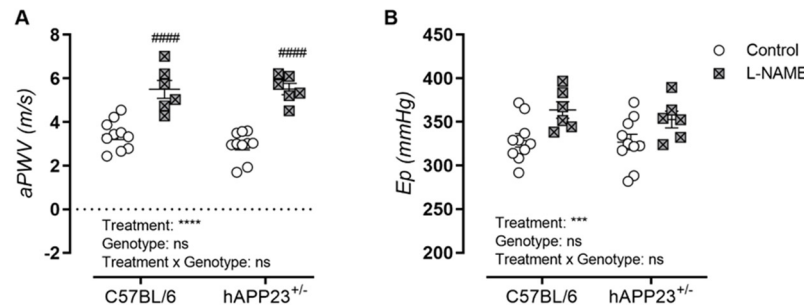


Figure 2. Assessment of in vivo and ex vivo AS. (A) In Vivo measurements of aPWV and (B) ex vivo measurements of Ep over a pressure range of 80–120 mmHg for (non)treated hAPP23+/- animals (control: n = 9; treated: n = 6) and C57BL/6 littermates (control: n = 10; treated: n = 6). Factorial ANOVA for the factor's 'Treatment', 'Genotype' and 'Treatment × Genotype', *** p < 0.001, **** p < 0.0001, with a Tukey post-hoc test for differences between (un)treated measurements per genotype, ##### p < 0.0001. Non-significant results are indicated as 'ns'. Data are presented as mean ± SEM.

3.4. L-NAME Treatment Worsens Spatiotemporal Learning and Memory Equally in hAPP23+/- and C57BL/6 Mice

A significant effect of the L-NAME treatment and the percentual presence of tested animals in each MWM quadrant was noticeable for hAPP23+/- and C57BL/6 animals, whereby L-NAME treated animals knew a more randomized presence in the MWM compared to untreated controls (Figure 3A). This finding was also observed after Dirichlet analysis of the MWM probe trial performances revealing a more randomized presence of L-NAME treated hAPP23+/- and C57BL/6 animals (Figure 3B).

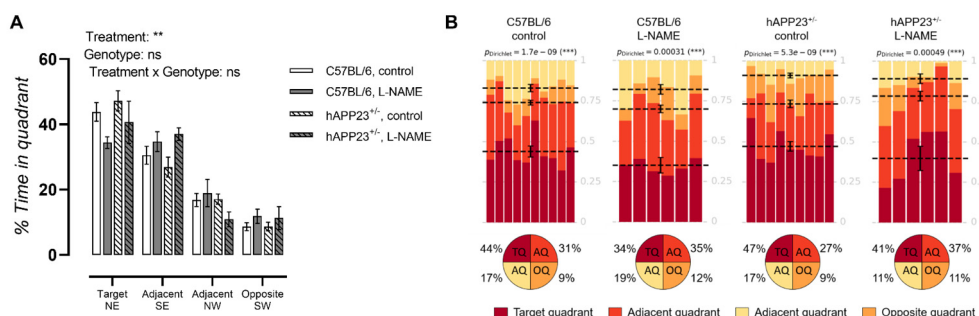


Figure 3. MWM probe trial results. (A) MWM probe trials of (un)treated hAPP23+/- animals (untreated: n = 9; treated: n = 6) and C57BL/6 littermates (untreated: n = 10; treated: n = 6). Factorial ANOVA for the factor's 'Quadrant × treatment', 'Quadrant × genotype', 'Quadrant × treatment × genotype', ** p < 0.01, *** p < 0.001. Non-significant results are indicated as 'ns'. Data are presented as mean ± SEM. (B) Statistical Dirichlet distributions of probe trial performances per tested group. Dirichlet distributions were calculated as previously described [27]. Each column represents the probe trial performance of a single animal and each color represents a different quadrant. Mean values for the fraction of time spent in each quadrant are represented by a dotted line with respective error bars for SEM. Average percentages of time spent in each quadrant are represented in pie charts beneath the calculated heatmap of each group.

3.5. L-NAME Treatment Does Not Affect Cerebral Amyloid Load in hAPP23^{+/−} Animals

Cerebral amyloidosis was assessed via histological analysis of the ventral hippocampus and cortex of all animals. Overall, the L-NAME treatment did not result in a significantly increased amyloid load in both the ventral hippocampus (Figure 4A) and cortex of hAPP23^{+/−} mice (Figure 4B). A decreased trend could be observed in the ventral cerebral cortex for L-NAME treated hAPP23^{+/−} mice compared to untreated hAPP23^{+/−} mice, which the authors attribute to the large distribution of data points.

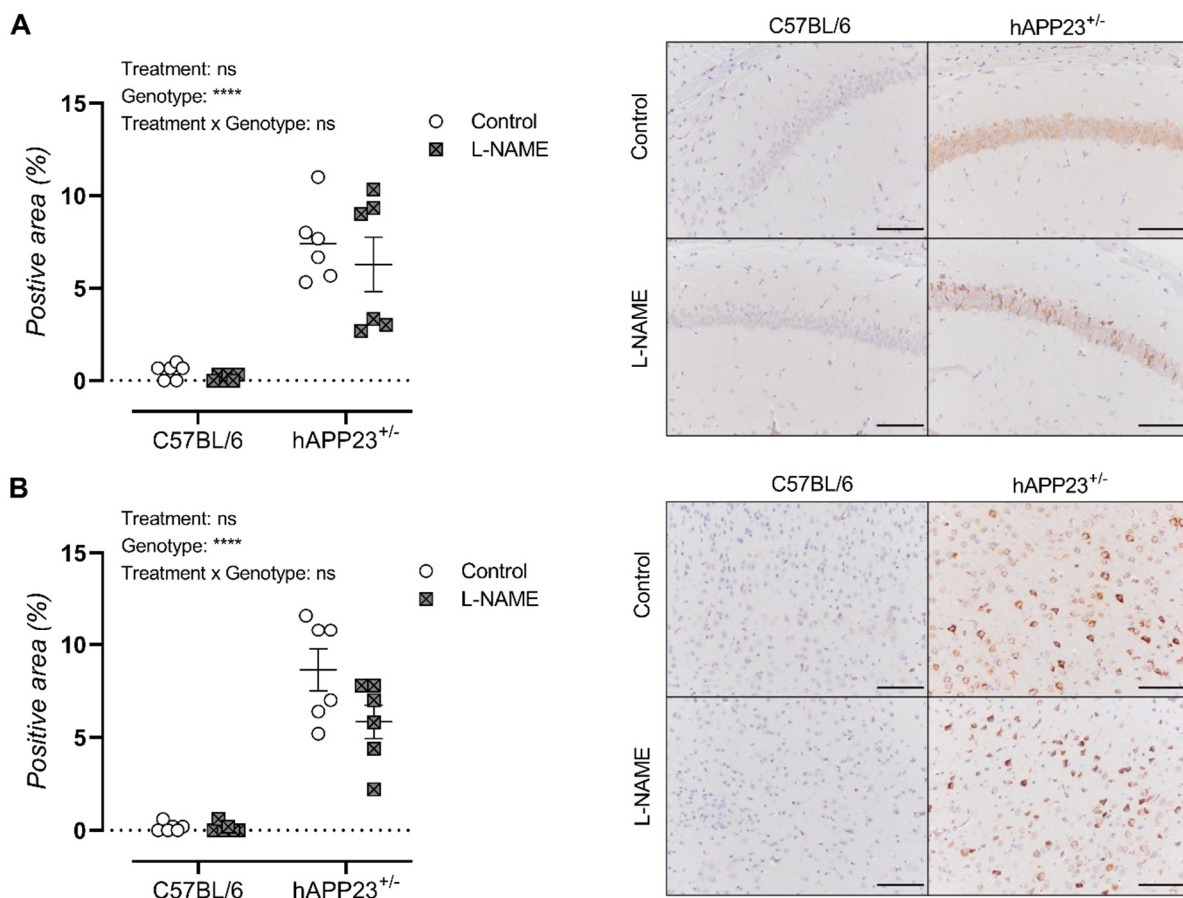


Figure 4. Histological assessment of cerebral amyloidosis in (A) the ventral hippocampus and (B) ventral cerebral cortex of un-treated and L-NAME treated hAPP23^{+/−} (untreated: n = 6; treated: n = 6) and C57BL/6 (untreated: n = 6; treated: n = 6) brains. Factorial ANOVA for the factor's 'Treatment', 'Genotype', 'Treatment × Genotype', **** p < 0.001. Non-significant results are indicated as 'ns'. Data are presented as mean ± SEM. Scale bars indicate 100 μm.

4. Discussion

In the current study, the assessment of in vivo and ex vivo AS revealed a significant increase in aPWV and Ep values in L-NAME-treated mice. These findings are consistent with prior research in rodent models of NO dysfunction [28,29] and align with observations in patients where treatment with an NOS messenger RNA activator led to improvements in AS [30]. Additionally, we observed indications of hypertrophic cardiomyopathy in the L-NAME-treated C57BL/6 and hAPP23^{+/−} mice. Notably, L-NAME treated hAPP23^{+/−} mice exhibited a substantial increase in IVRT measurements when compared to (un)treated C57BL/6 animals. These results underscore the crucial role of NOS activity in regulating both AS and cardiac function.

The impact of L-NAME on hippocampal-dependent spatiotemporal learning and memory was assessed using the MWM test in both C57BL/6 and hAPP23^{+/−} mice. Our findings revealed a significant decline in learning and memory performance in both groups

after 16 weeks of L-NAME treatment, highlighting the pivotal role of nNOS in cardiovascular and neurological pathophysiology. This neurobehavioral effect was similarly observed in hAPP23+/- mice. However, we did not detect a significant increase in amyloid load in the brains of hAPP23+/- mice following L-NAME treatment. It is important to note that data variability was notable in both hippocampal and cortical tissue samples of hAPP23+/- mice, likely due to the relatively small sample size. We acknowledge this as a limitation and stress the need for more comprehensive studies on cerebral amyloidosis resulting from L-NAME treatment. Nevertheless, similar findings were obtained in a hybrid AD murine model (APPSwDI/NOS2-/-), which displayed impaired spatial memory compared to APPSwDI mice but had unaltered cerebral A β levels. Additionally, APPSwDI/NOS2-/- mice exhibited extensive tau pathology associated with regions of dense microvascular amyloid deposition [31]. Other research has also demonstrated increased cerebrovascular A β in 18-month-old eNOS+/- mice [14], impairment in neurovascular coupling mediated by a reduction in nNOS activity *in vivo* [32], and promotion of tau phosphorylation in neuronal tissue by loss of eNOS [17].

Under normal physiological conditions, nNOS facilitates the synthesis of neuronal NO from L-arginine. It is important to note that not all neurons express nNOS. In vulnerable brain regions associated with AD, such as the hippocampus and cortex, nNOS is primarily found in specific subpopulations of γ -aminobutyric acid (GABA)-releasing neurons [33,34]. In these neurons, nNOS plays a role in regulating local blood flow [35], seizures [36], and epileptiform activities [37]. Under conditions of oxidative stress, where the levels of its cofactor tetrahydrobiopterin are reduced, nNOS may produce additional superoxide anions, which can lead to the formation of peroxynitrite [38]. AD-affected brains have been reported to exhibit decreased levels of tetrahydrobiopterin [39], rendering them more susceptible to nitro-oxidative stress. Furthermore, neurons expressing nNOS have been observed to be highly vulnerable to A β -induced neurodegeneration in various regions of AD-affected brains [40]. These findings suggest a potential role for nNOS dysregulation in the degeneration of GABAergic neurons in AD. Nevertheless, the precise molecular mechanisms underlying this process remain unclear, and further research is essential to elucidate the role and differences in nNOS activity in GABAergic neurons between healthy and AD-affected brains.

It is important to acknowledge that L-NAME can penetrate the blood-brain barrier through arginine transporters expressed at the blood-brain barrier [41]. With a 72% likelihood of crossing the blood-brain barrier [42], it is plausible that the cognitive decline observed in this research following L-NAME treatment could be partially attributed to the inhibition of nNOS in the brain, irrespective of its impact on AS. Given the relatively low dose of L-NAME administered to the mice in this study [19,20] and its lower inhibitory constant (K_i) value for nNOS compared to eNOS and iNOS [43,44], it is probable that nNOS activity was indeed inhibited in the brain. However, we did not conduct an in-depth analysis of NO levels or the transcriptional and translational NOS expression in the specific brain regions studied. Therefore, we suggest conducting more comprehensive studies to thoroughly assess NO levels, NOS expressions, and total antioxidant levels for a better understanding of the subject.

5. Conclusions

In conclusion, our findings demonstrate that non-selective inhibition of NOS activity with L-NAME induces arterial stiffness and a decrease in hippocampal-dependent spatiotemporal learning and memory to the same extent in control and AD mice, highlighting the importance of nNOS in cognitive aging independent of a genetic AD predisposition.

Author Contributions: J.O.H. and E.C. conducted the experiments and analysis of data; P.P.D.D. delivered acquisition of financial support for the project leading to this publication; G.R.Y.D.M., D.V.D. and P.P.D.D. critically reviewed and edited the manuscript; J.O.H., D.V.D. and G.R.Y.D.M. contributed to the conceptualization of the experiment and the writing of the original draft. All authors have read and agreed to the published version of the manuscript.

Funding: This work was supported by the University of Antwerp (GOA-BOF, grant 33931), the Research Foundation-Flanders, the Medical Research Foundation Antwerp, Neurosearch Antwerp, and the Hercules Foundation (grant N° AU-HA/13/03).

Institutional Review Board Statement: Experiments were approved by the Animal Ethics Committee of the University of Antwerp (ECD approval No. 2017/53, approved on 26 July 2017) and were conducted in accordance with the EU Directive 2010/63/EU and in accordance with the Animal Research: Reporting of In Vivo Experiments (ARRIVE) Guidelines.

Informed Consent Statement: The authors declare that they have no known competing financial interests or personal relationships that could have appeared to influence the work reported in this manuscript.

Data Availability Statement: The data presented in this study are available upon reasonable request from the corresponding author.

Acknowledgments: The authors want to thank Mandy Vermont and Hermine Fret for the technical support.

Conflicts of Interest: The authors declare that they have no known competing financial interest or personal relationship that could have appeared to influence the work reported in this manuscript.

References

1. Iulita, M.F.; Noriega de la Colina, A.; Girouard, H. Arterial stiffness, cognitive impairment and dementia: Confounding factor or real risk? *J. Neurochem.* **2018**, *144*, 527–548. [[CrossRef](#)] [[PubMed](#)]
2. van Sloten, T.T.; Protogerou, A.D.; Henry, R.M.; Schram, M.T.; Launer, L.J.; Stehouwer, C.D. Association between arterial stiffness, cerebral small vessel disease and cognitive impairment: A systematic review and meta-analysis. *Neurosci. Biobehav. Rev.* **2015**, *53*, 121–130. [[CrossRef](#)] [[PubMed](#)]
3. Hendrickx, J.O.; Martinet, W.; Van Dam, D.; De Meyer, G.R. Inflammation, Nitro-Oxidative Stress, Impaired Autophagy, and Insulin Resistance as a Mechanistic Convergence between Arterial Stiffness and Alzheimer’s Disease. *Front. Mol. Biosci.* **2021**, *8*, 185. [[CrossRef](#)] [[PubMed](#)]
4. O’Rourke, M.F.; Safar, M.E. Relationship between aortic stiffening and microvascular disease in brain and kidney: Cause and logic of therapy. *Hypertension* **2005**, *46*, 200–204. [[CrossRef](#)] [[PubMed](#)]
5. Rabkin, S.W. Arterial stiffness: Detection and consequences in cognitive impairment and dementia of the elderly. *J. Alzheimer’s Dis.* **2012**, *32*, 541–549. [[CrossRef](#)] [[PubMed](#)]
6. Moon, S.W.; Byun, M.S.; Yi, D.; Lee, J.H.; Jeon, S.Y.; Lee, Y.; Kee, B.S.; Lee, D.Y.; Group, K.R. The Ankle–Brachial Index Is Associated with Cerebral β-Amyloid Deposition in Cognitively Normal Older Adults. *J. Gerontol. Ser. A* **2019**, *74*, 1141–1148. [[CrossRef](#)]
7. Hughes, T.M.; Wagenknecht, L.E.; Craft, S.; Mintz, A.; Heiss, G.; Palta, P.; Wong, D.; Zhou, Y.; Knopman, D.; Mosley, T.H. Arterial stiffness and dementia pathology: Atherosclerosis Risk in Communities (ARIC)-PET Study. *Neurology* **2018**, *90*, e1248–e1256. [[CrossRef](#)]
8. Pasha, E.P.; Rutjes, E.; Tomoto, T.; Tarumi, T.; Stowe, A.; Claassen, J.; Munro Cullum, C.; Zhu, D.C.; Zhang, R. Carotid Stiffness is Associated with Brain Amyloid-beta Burden in Amnestic Mild Cognitive Impairment. *J. Alzheimers Dis.* **2020**, *74*, 925–935. [[CrossRef](#)]
9. Hughes, T.M.; Kuller, L.H.; Barinas-Mitchell, E.J.; McDade, E.M.; Klunk, W.E.; Cohen, A.D.; Mathis, C.A.; DeKosky, S.T.; Price, J.C.; Lopez, O.L. Arterial stiffness and β-amyloid progression in nondemented elderly adults. *JAMA Neurol.* **2014**, *71*, 562–568. [[CrossRef](#)]
10. Hendrickx, J.O.; De Moudt, S.; Calus, E.; De Deyn, P.P.; Van Dam, D.; De Meyer, G.R. Long-Term Pharmacological Inhibition of the Activity of All NOS Isoforms Rather Than Genetic Knock-Out of Endothelial NOS Leads to Impaired Spatial Learning and Memory in C57BL/6 Mice. *Biomedicines* **2021**, *9*, 1905. [[CrossRef](#)]
11. Chiba, T.; Sakuma, K.; Komatsu, T.; Cao, X.; Aimoto, M.; Nagasawa, Y.; Shimizu, K.; Takahashi, M.; Hori, Y.; Shirai, K. Physiological role of nitric oxide for regulation of arterial stiffness in anesthetized rabbits. *J. Pharmacol. Sci.* **2019**, *139*, 42–45. [[CrossRef](#)] [[PubMed](#)]
12. Dubey, H.; Gulati, K.; Ray, A. Alzheimer’s Disease: A Contextual Link with Nitric Oxide Synthase. *Curr. Mol. Med.* **2020**, *20*, 505–515. [[CrossRef](#)] [[PubMed](#)]
13. Stefano, G.B.; Esch, T.; Ptacek, R.; Kream, R.M. Dysregulation of Nitric Oxide Signaling in Microglia: Multiple Points of Functional Convergence in the Complex Pathophysiology of Alzheimer Disease. *Med. Sci. Monit.* **2020**, *26*, e927739. [[CrossRef](#)] [[PubMed](#)]
14. Austin, S.A.; Katusic, Z.S. Partial loss of endothelial nitric oxide leads to increased cerebrovascular beta amyloid. *J. Cereb. Blood Flow. Metab.* **2020**, *40*, 392–403. [[CrossRef](#)] [[PubMed](#)]

15. Do, H.T.; Li, H.; Chreifi, G.; Poulos, T.L.; Silverman, R.B. Optimization of Blood–Brain Barrier Permeability with Potent and Selective Human Neuronal Nitric Oxide Synthase Inhibitors Having a 2-Aminopyridine Scaffold. *J. Med. Chem.* **2019**, *62*, 2690–2707. [CrossRef] [PubMed]
16. Wardlaw, J.M.; Doubal, F.N.; Valdes-Hernandez, M.; Wang, X.; Chappell, F.M.; Shuler, K.; Armitage, P.A.; Carpenter, T.C.; Dennis, M.S. Blood-brain barrier permeability and long-term clinical and imaging outcomes in cerebral small vessel disease. *Stroke* **2013**, *44*, 525–527. [CrossRef] [PubMed]
17. Austin, S.A.; Katusic, Z.S. Loss of Endothelial Nitric Oxide Synthase Promotes p25 Generation and Tau Phosphorylation in a Murine Model of Alzheimer’s Disease. *Circ. Res.* **2016**, *119*, 1128–1134. [CrossRef]
18. Sturchler-Pierrat, C.; Abramowski, D.; Duke, M.; Wiederhold, K.-H.; Mistl, C.; Rothacher, S.; Ledermann, B.; Bürki, K.; Frey, P.; Paganetti, P.A. Two amyloid precursor protein transgenic mouse models with Alzheimer disease-like pathology. *Proc. Natl. Acad. Sci. USA* **1997**, *94*, 13287–13292. [CrossRef]
19. Nagano, K.; Ishida, J.; Unno, M.; Matsukura, T.; Fukamizu, A. Apelin elevates blood pressure in ICR mice with L-NAME-induced endothelial dysfunction. *Mol. Med. Rep.* **2013**, *7*, 1371–1375. [CrossRef]
20. Suda, O.; Tsutsui, M.; Morishita, T.; Tanimoto, A.; Horiuchi, M.; Tasaki, H.; Huang, P.L.; Sasaguri, Y.; Yanagihara, N.; Nakashima, Y. Long-term treatment with N ω -nitro-L-arginine methyl ester causes arteriosclerotic coronary lesions in endothelial nitric oxide synthase-deficient mice. *Circulation* **2002**, *106*, 1729–1735. [CrossRef]
21. Underwood, W.; Anthony, R. AVMA Guidelines for the Euthanasia of Animals: 2020 Edition. *Retrieved March* **2013**, *30*.
22. Kilkenny, C.; Browne, W.; Cuthill, I.; Emerson, M.; Altman, D.G. The ARRIVE guidelines. *ResqartoCom* **2010**, *8*, 1–2.
23. Van Dam, D.; d’Hooge, R.; Staufenbiel, M.; Van Ginneken, C.; Van Meir, F.; De Deyn, P.P. Age-dependent cognitive decline in the APP23 model precedes amyloid deposition. *Eur. J. Neurosci.* **2003**, *17*, 388–396. [CrossRef] [PubMed]
24. Van Dam, D.; Lenders, G.; De Deyn, P.P. Effect of Morris water maze diameter on visual-spatial learning in different mouse strains. *Neurobiol. Learn. Mem.* **2006**, *85*, 164–172. [CrossRef] [PubMed]
25. Feng, M.; Whitesall, S.; Zhang, Y.; Beibel, M.; Alecy, L.D.; DiPetrillo, K. Validation of volume–pressure recording tail-cuff blood pressure measurements. *Am. J. Hypertens.* **2008**, *21*, 1288–1291. [CrossRef]
26. Di Lascio, N.; Stea, F.; Kusmic, C.; Sicari, R.; Faita, F. Non-invasive assessment of pulse wave velocity in mice by means of ultrasound images. *Atherosclerosis* **2014**, *237*, 31–37. [CrossRef]
27. Maugard, M.; Doux, C.; Bonvento, G. A new statistical method to analyze Morris Water Maze data using Dirichlet distribution. *F1000Research* **2019**, *8*, 1601. [CrossRef]
28. Leloup, A.J.; Fransen, P.; Van Hove, C.E.; Demolder, M.; De Keulenaer, G.W.; Schrijvers, D.M. Applanation tonometry in mice: A novel noninvasive technique to assess pulse wave velocity and arterial stiffness. *Hypertension* **2014**, *64*, 195–200. [CrossRef]
29. Isabelle, M.; Simonet, S.; Ragonnet, C.; Sansilvestri-Morel, P.; Clavreul, N.; Vayssettes-Courchay, C.; Verbeuren, T.J. Chronic reduction of nitric oxide level in adult spontaneously hypertensive rats induces aortic stiffness similar to old spontaneously hypertensive rats. *J. Vasc. Res.* **2012**, *49*, 309–318. [CrossRef]
30. Park, S.U.; Jung, W.S.; Moon, S.K.; Ko, C.N.; Cho, K.H.; Kim, Y.S.; Bae, H.S. Chunghyul-Dan (Qingxie-dan) improves arterial stiffness in patients with increased baPWV. *Am. J. Chin. Med.* **2006**, *34*, 553–563. [CrossRef]
31. Wilcock, D.M.; Lewis, M.R.; Van Nostrand, W.E.; Davis, J.; Previti, M.L.; Gharkholonarehe, N.; Vitek, M.P.; Colton, C.A. Progression of amyloid pathology to Alzheimer’s disease pathology in an amyloid precursor protein transgenic mouse model by removal of nitric oxide synthase 2. *J. Neurosci.* **2008**, *28*, 1537–1545. [CrossRef] [PubMed]
32. Van Skike, C.E.; Hussong, S.A.; Banh, A.; Galvan, V. Nitric Oxide Synthase Dysfunction Underlies Cerebrovascular Deficits in a Mouse Model of Tauopathy. *Innov. Aging* **2019**, *3* (Suppl. S1), S91. [CrossRef]
33. Gasulla, J.; Calvo, D.J. Enhancement of tonic and phasic GABAergic currents following nitric oxide synthase inhibition in hippocampal CA1 pyramidal neurons. *Neurosci. Lett.* **2015**, *590*, 29–34. [CrossRef] [PubMed]
34. Tricoire, L.; Tania, V. Neuronal nitric oxide synthase expressing neurons: A journey from birth to neuronal circuits. *Front. Neural Circuits* **2012**, *6*, 82. [CrossRef] [PubMed]
35. Perrenoud, Q.; Rossier, J.; Férezou, I.; Geoffroy, H.; Gallopin, T.; Vitalis, T.; Rancillac, A. Activation of cortical 5-HT3 receptor-expressing interneurons induces NO mediated vasodilatations and NPY mediated vasoconstrictions. *Front. Neural. Circuits* **2012**, *6*, 50. [CrossRef] [PubMed]
36. Gholipour, T.; Ghasemi, M.; Riazi, K.; Ghaffarpour, M.; Dehpour, A.R. Seizure susceptibility alteration through 5-HT3 receptor: Modulation by nitric oxide. *Seizure* **2010**, *19*, 17–22. [CrossRef] [PubMed]
37. Rajasekaran, K.; Jayakumar, R.; Venkatachalam, K. Increased neuronal nitric oxide synthase (nNOS) activity triggers picrotoxin-induced seizures in rats and evidence for participation of nNOS mechanism in the action of antiepileptic drugs. *Brain Res.* **2003**, *979*, 85–97. [CrossRef] [PubMed]
38. Pall, M.L. Nitric oxide synthase partial uncoupling as a key switching mechanism for the NO/ONOO–cycle. *Med. Hypotheses* **2007**, *69*, 821–825. [CrossRef]
39. Barford, P.; Blair, J.; Eggar, C.; Hamon, C.; Morar, C.; Whitburn, S. Tetrahydrobiopterin metabolism in the temporal lobe of patients dying with senile dementia of Alzheimer type. *J. Neurol. Neurosurg. Psychiatry* **1984**, *47*, 736–738. [CrossRef]
40. Thorns, V.; Hansen, L.; Masliah, E. nNOS expressing neurons in the entorhinal cortex and hippocampus are affected in patients with Alzheimer’s disease. *Exp. Neurol.* **1998**, *150*, 14–20. [CrossRef]

41. Montaser, A.B.; Jarvinen, J.; Löffler, S.; Huttunen, J.; Auriola, S.; Lehtonen, M.; Jalkanen, A.; Huttunen, K.M. L-Type Amino Acid Transporter 1 Enables the Efficient Brain Delivery of Small-Sized Prodrug across the Blood–Brain Barrier and into Human and Mouse Brain Parenchymal Cells. *ACS Chem. Neurosci.* **2020**, *11*, 4301–4315. [[CrossRef](#)] [[PubMed](#)]
42. Majzúnová, M.; Pakanová, Z.; Kvasnička, P.; Bališ, P.; Čačányiová, S.; Dovinová, I. Age-dependent redox status in the brain stem of NO-deficient hypertensive rats. *J. Biomed. Sci.* **2017**, *24*, 72. [[CrossRef](#)] [[PubMed](#)]
43. Reif, D.W.; McCreedy, S.A. N-nitro-L-arginine and N-monomethyl-L-arginine exhibit a different pattern of inactivation toward the three nitric oxide synthases. *Arch. Biochem. Biophys.* **1995**, *320*, 170–176. [[CrossRef](#)] [[PubMed](#)]
44. Pfeiffer, S.; Leopold, E.; Schmidt, K.; Brunner, F.; Mayer, B. Inhibition of nitric oxide synthesis by NG-nitro-L-arginine methyl ester (L-NAME): Requirement for bioactivation to the free acid, NG-nitro-L-arginine. *Br. J. Pharmacol.* **1996**, *118*, 1433–1440. [[CrossRef](#)]

Disclaimer/Publisher’s Note: The statements, opinions and data contained in all publications are solely those of the individual author(s) and contributor(s) and not of MDPI and/or the editor(s). MDPI and/or the editor(s) disclaim responsibility for any injury to people or property resulting from any ideas, methods, instructions or products referred to in the content.